J Mater Sci (2006) 41:7760–7768
DOI 10.1007/s10853-006-0406-z

Some aspects of the anisotropy of grain boundary segregation and wetting

P. Wynblatt · D. Chatain · Y. Pang

Received: 20 February 2006 / Accepted: 3 May 2006 / Published online: 24 October 2006

Abstract A recently developed model of grain boundary (GB) segregation, in terms of the five macroscopic parameters of GB orientation, has been exercised to explore the anisotropy of GB segregation. The five macroscopic GB orientation parameters are defined by means of the orientations of the two crystallographic planes that terminate the crystals on either side of the GB, and a twist angle. Some important conclusions include the following: (a) the composition of a boundary depends on all five parameters of GB orientation, (b) the segregation profile across a GB depends on the two planes which terminate the adjacent crystals, (c) the composition profile across GB's terminated by identical crystallographic planes is symmetric, but is asymmetric when GB's are terminated by different planes, and (d) the strength of the segregation on one side of a GB influences the extent of segregation on the other. Some experimental results on Nb-doped TiO_2 are presented in order to verify above predicted trends. In addition, it is shown that the model predicts the possibility of anisotropic GB wetting transitions as two-phase coexistence is approached.

P. Wynblatt (✉) · Y. Pang
Department of Materials Science and Engineering, Carnegie Mellon University, Pittsburgh, PA 15213-3890, USA
e-mail: pw01@andrew.cmu.edu

D. Chatain
Centre de Recherche en Matière Condensée et Nanosciences-CNRS, Laboratoire Propre du CNRS associé aux Universités d'Aix-Marseille 2 et 3, campus de Luminy, case 913, 13288 Marseille cedex 9, France

Present Address:
Y. Pang
Sort/Test Technology Development, Intel Corporation, 3585 SW 198th Ave, Aloha, OR 97007, USA

Introduction

Grain boundary (GB) segregation has been studied for close to half a century, and continues to be the subject of considerable interest, because of the important role it plays in the properties of polycrystalline aggregates. With the recent advent of orientation imaging microscopy (OIM), the ability to characterize GB's in polycrystals has been considerably enhanced, as has the capability for probing the anisotropic character of GB's. Whereas OIM cannot be used to investigate GB segregation phenomena directly, it can be used, for example, to study the changes in GB orientation distribution that result from the segregation of GB-active solutes. Furthermore, OIM can be used to advantage, in conjunction with traditional methods for investigating GB segregation, such as Auger electron spectroscopy, to hasten the acquisition of moderately large data sets on GB segregation anisotropy [1, 2]. The interpretation of such data sets requires some novel approaches to the modeling of GB segregation anisotropy.

Whereas most of the modeling of the anisotropic behavior of GB's has been performed in the past by atomistic computer simulation [3–6], it is currently impractical to use this approach to model extensive experimentally derived data sets on large angle GB's with arbitrary values of the five macroscopic parameters

of GB orientation. Recently, however, an analytical model of the anisotropy of GB segregation has been developed for the case of GB's in FCC alloys [7]. Simulations give precise predictions, but for a range of experimental conditions that limit their practical applications, the model is able to provide useful information on trends in GB segregation over the 5-dimensional space of GB orientation. The purpose of this paper is to illustrate the capabilities of the model by presenting examples of its predictions.

Beyond conventional GB segregation phenomena, the GB segregation model also predicts conditions under which wetting transitions can occur at GB's. This is of some interest, as there has been a recent increase in both theoretical [8–11] and experimental [12–14] activity surrounding phenomena related to GB wetting, driven in part by a renewal of technological concerns regarding liquid metal embrittlement as well as the observation of glassy intergranular films in ceramics. Thus, we will also report some preliminary results obtained by the GB segregation model on the topic of GB wetting transitions.

Anisotropic GB segregation model

The detailed description of the model has been given elsewhere [7]; here we provide only a brief outline. The model is based on the regular solution formalism of interfacial segregation [15–17], in which the energies of the two crystals adjacent to GB are described in terms of nearest neighbor bonds. Each crystal consists of atoms located on the lattice points of planes of orientation (*hkl*) terminating at the GB, thus no structural relaxation is permitted. In general, the two crystals will be terminated by different (*hkl*) planes (referred to as $(hkl)_1$ and $(hkl)_2$), and will be rotated with respect to each other by a twist angle, ϕ, about an axis perpendicular to the GB plane. The five macroscopic orientation parameters of the GB are then taken to be the two variables required to define each of the two terminating (*hkl*) planes, and the twist angle. This method of defining the macroscopic parameters has been referred to as the *interface plane scheme* [3–5].

The indices of the terminating planes must be chosen such that $h \geq k \geq l$ and be reduced to the lowest integers. (*hkl*) planes in each crystal are numbered by an index *i*, where $i = 1$ identifies the terminating plane at the GB. It is also necessary to define a second index, *j*, which counts the planes from any given plane *i*. The maximum value of *j* is denoted by J_{max}, and represents the farthest plane containing nearest neighbors of atoms in the *i*th plane. In FCC crystals J_{max} is defined by: $J_{max}, = (h + k)/2$ when *h*, *k*, and *l*, are all odd, and $J_{max} = (h + k)$ for mixed *h*, *k*, and *l*. The indices *i* and *j* are illustrated in the schematic of Fig. 1 and are also explained in greater detail in a pair of papers by Lee and Aaronson [18, 19].

We consider an FCC binary A–B substitutional solid solution in which the solute species is taken to be component B. The composition of the *i*th atomic plane on one side of the GB adopts the usual regular solution form:

$$\ln \frac{x^i}{1-x^i} = \ln \frac{x}{1-x} - \frac{\Delta H^i_{\mathrm{seg}}}{RT} \tag{1}$$

where x^i and x are the atomic fractions of the component B in the *i*th atomic plane and in the bulk, respectively, and $\Delta H^i_{\mathrm{seg}}$ is the enthalpy of segregation to the *i*th plane, which includes both nearest neighbor bond as well as elastic strain energy terms.

One important difference between GB's and crystalline surfaces, in the context of a nearest neighbor bond model, is that the relative locations of atoms across a GB are not compatible with nearest neighbor distances. At a crystalline surface, the surface energy depends in part on the energy of the dangling bonds. In contrast, at a GB, a certain fraction of the dangling bonds of the atoms on one side of the GB will be reconnected to the atoms on the other side of the GB. A parameter, *P*, is used to represent the fraction of

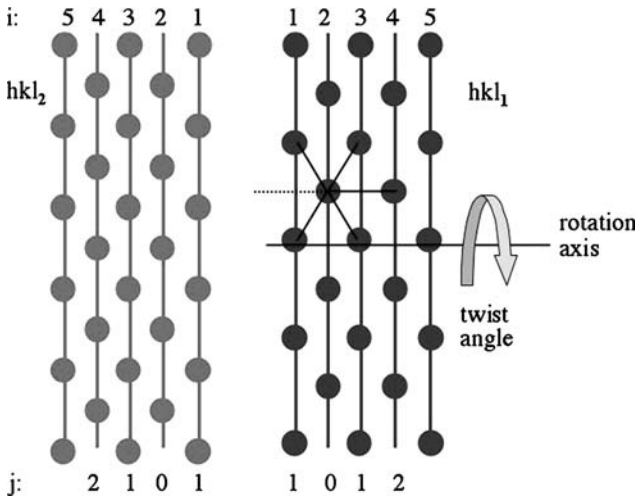

Fig. 1 Schematic of GB formed by bringing together two crystals terminated crystallographic planes $(hkl)_1$ and $(hkl)_2$, and twisting by an angle ϕ about an axis perpendicular to GB plane. The indices *i* number the planes of the two crystals away from the GB. The indices *j* are illustrated here for the planes $i = 2$. A dangling bond from an atom in plane $i = 2$ is shown as a dashed line. Dangling bonds are reconnected to the other side of the GB with probability *P* (see text)

broken bonds at a surface that are reconnected to the other side of the GB when two surfaces are brought together to form a GB. P depends on the Miller indices of the GB terminating planes, as well as the twist angle. A detailed derivation of that parameter has been given previously [7].

The expressions for the equilibrium atom fractions of each atom layer in the vicinity of each side of the GB will have the form of Eq. 1, in which the heat of segregation of the ith atom plane is given by:

$$\Delta H^i_{\text{seg}} = 2\omega\left[zx - z^i x^i - \sum_{j=1}^{J_{\max}} z^j x^{i+j} - \sum_{j=1}^{i-1} z^j x^{i-j} - P\sum_{j=i}^{J_{\max}} z^j x' - \frac{1}{2}(1-P)\sum_{j=i}^{J_{\max}} z^j\right] - \frac{1}{2}(1-P)(\varepsilon_{BB}-\varepsilon_{AA})\sum_{j=i}^{J_{\max}} z^j - \Delta E^i_{el} \quad (2)$$

for $i \le J_{\max}$, i.e. planes with less than the bulk coordination, and by:

$$\Delta H^i_{\text{seg}} = 2\omega\left[zx - z^i x^i - \sum_{j=1}^{J_{\max}} z^j\left(x^{i+j} + x^{i-j}\right)\right] - \Delta E^i_{el} \quad (3)$$

for the planes $i > J_{\max}$. Here ϵ_{AA} and ϵ_{BB} are the nearest neighbor bond energies in pure A and B, respectively, ω is the regular solution constant, ΔE^i_{el} is the bulk elastic energy of a solute atom that is dissipated in layer i [7], z^i is the number of nearest neighbors of an atom in the ith plane which also lie in the ith plane, and z^j is the number of nearest neighbors of an atom in the ith plane which lie in the jth plane (such that the total coordination of an atom is given by $z = z^i + 2\sum_{j=1}^{J_{\max}} z^j$), and x' is a weighted average of the near-GB composition of the crystal on the other side of the boundary, given by $x' = \sum_{i=1}^{J_{\max}} \sum_{j=i}^{J_{\max}} z^j x^i \Big/ \sum_{i=1}^{J_{\max}} \sum_{j=i}^{J_{\max}} z^j$.

It should be noted that the equation for the composition of a given plane i, obtained by substituting ΔH^i_{seg} into Eq. 1, is transcendental, and must be solved for the equilibrium plane composition by numerical methods. In addition, the equilibrium composition of a grain boundary must be obtained iteratively. The compositions of all planes on both sides of the GB are initially set to the bulk composition, and the compositions on one side are computed. This allows a first approximation of x' for the first side of the GB to be calculated, and used for the computation of compositions on the second side. The procedure is continued until compositions on both sides converge.

Validation of the model

Unfortunately there are no suitable experimental data sets on segregation to general GB's in FCC alloys that can be used to test the predictions of the above model. Nevertheless, it has been possible to test the model [7] against data sets for special GB's obtained by Udler and Seidman [20, 21], who conducted a series of consistent Monte Carlo simulations, in conjunction with embedded atom method (EAM) potentials [22], on four alloys. These authors investigated the compositions of symmetric <100> twist GB's in Pt–1at%Au, Au–1at% Pt, Pt–3 at% Ni and Ni–3at%Pt. As an example, Fig. 2a shows a comparison between the predictions of the model with the simulation results for the case of Pt–1at%Au, in the form of a plot of segregation (or adsorption) versus twist angle [7]. The figure displays good qualitative agreement, and reasonable quantitative agreement, between model and simulation results, both in terms of the dependence of segregation on twist angle, as well as on the effects of temperature on adsorption. Figure 2b shows a comparison of the plane-by-plane composition profile across the most highly segregated GB at a twist angle of ~43°. Here again, good agreement is obtained. Comparable agreement was also found in similar comparisons with the three other alloys for which simulations were performed, thereby verifying that the model produces predictions that are compatible with the results of discrete atomistic calculations.

Predictions of GB segregation anisotropy and some comparisons with experiment

Selected model predictions

In most of the following illustrations of model trends, we use parameters obtained from embedded atom method potentials for the Pt–Au system [22], and apply them to computations of segregation in Pt–Au alloys dilute in Au. This is the same choice of parameters as in the case of Fig. 2, where model predictions were found to be in good agreement with computer simulations. The parameters include the pure component bond energies; $\epsilon_{\text{PtPt}} = -38237$ J/mol and $\epsilon_{\text{AuAu}} = -21273$ J/mol (computed from the (100) surface

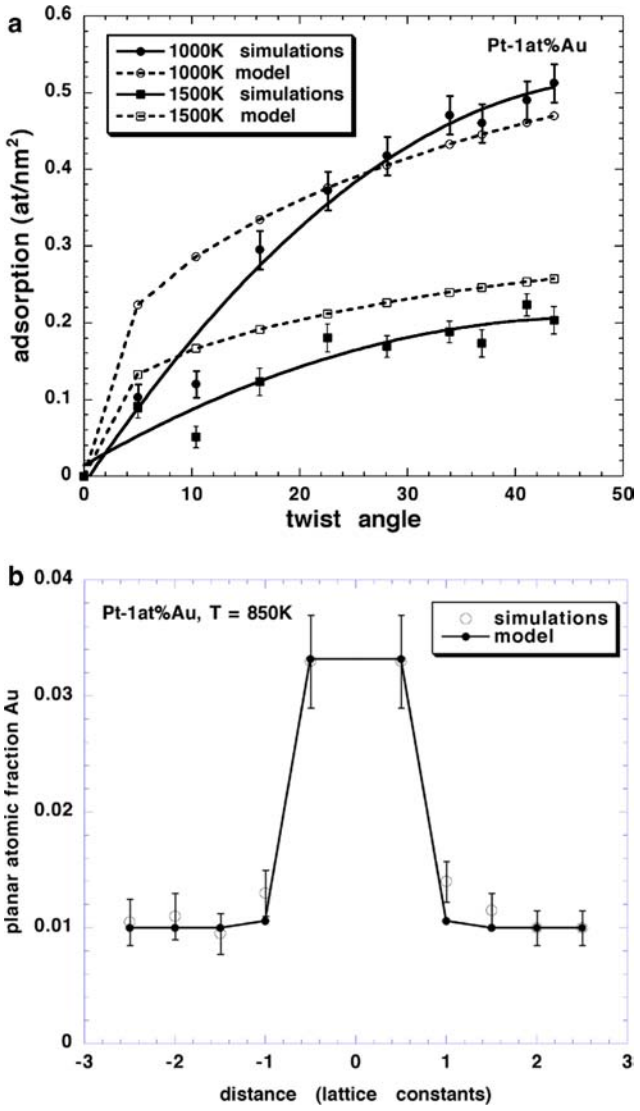

Fig. 2 Comparison between the GB segregation model and the computer simulations of Udler and Seidman in Pt-1at%Au [20, 21]. (**a**) Dependence of GB adsorption on twist angle for symmetric <100> twist GB's, and (**b**) composition profile of Au across the GB with a twist angle of 43.6° (after ref [7])

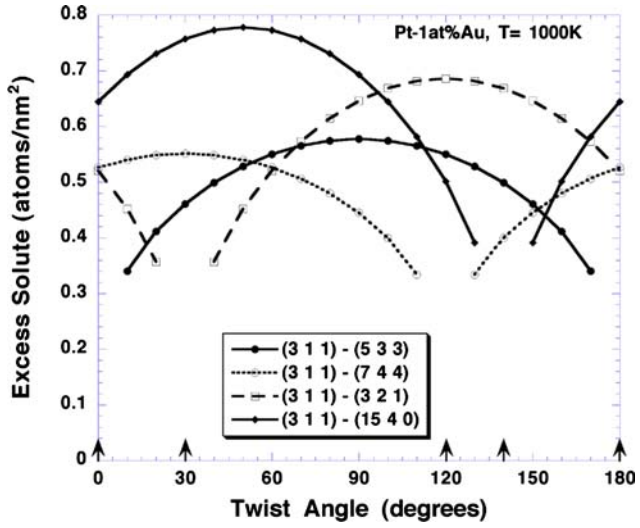

Fig. 3 Examples of model predictions for asymmetric twist GB's, as a function of twist angle, for a Pt-1 at%Au alloy at 1000 K. All GB's are terminated by a (311) plane on one side, and by four different (*hkl*) planes on the other. Arrows indicate the location of cusps [7]

energies), the regular solution constant ω = 562 J/mol, the lattice constants a_{Pt} = 0.392 nm and a_{Au} = 0.405 nm, the bulk modulus K_{Au} = 1.67 ergs/cm^3 and the shear modulus G_{Pt} = 0.68 ergs/cm^3 [22].

Figure 3 displays the composition at 1000 K of selected GB's in Pt–1at%Au. The figure shows the compositions of four GB's, all terminated by a (311) plane on one side, and four different (*hkl*) planes on the other, as a function of twist angle. The (311) plane lies on the (100)–(111) edge of the stereographic triangle. The other sides of the four GB's are terminated respectively by the (533), which also lies on the (100)–(111) edge, the (744) plane, which lies along the (110)–(111) edge, the (15 4 0) plane which lies on the (100)–(110) edge, and the (321) which lies near the center of the triangle. Thus, the GB orientations are well distributed over the orientation space. The location of energy cusps, that arise for these GB's at specific values of twist angle, are indicated by arrows on the horizontal axis of the figure. Although the model correctly predicts the values of twist angle at which energy cusps are located, the depth of energy cusps is calculated rather crudely [10, 11]. As a result, cusp values of the composition have been omitted. Nevertheless, Fig. 3 indicates that the magnitude of compositional anisotropy of the GB's in dilute Pt–Au alloys at 1000 K ranges over a factor of about three for the selected GB's. Of course, a larger anisotropy would be expected over the whole GB orientation space or at different temperatures. Furthermore, the range of compositional anisotropy could be larger or smaller than in the specific case of the Pt–1at%Au alloy used here for the purposes of illustration.

Displaying GB compositional information for the complete five-parameter space is impractical, as it requires a very large number of figures. Thus, from now on, we shall display results limited to a four-parameter space, in which the twist angle parameter has been selected so as to correspond to the maximum value of GB composition for a given pair of terminating GB planes.

To begin with, we show some effects related to the anisotropy of the composition profile across GB's by displaying the results of sample calculations in Fig. 4. In Fig. 4a, we show the profiles across four GB's consisting of identical pairs of terminating planes, namely:

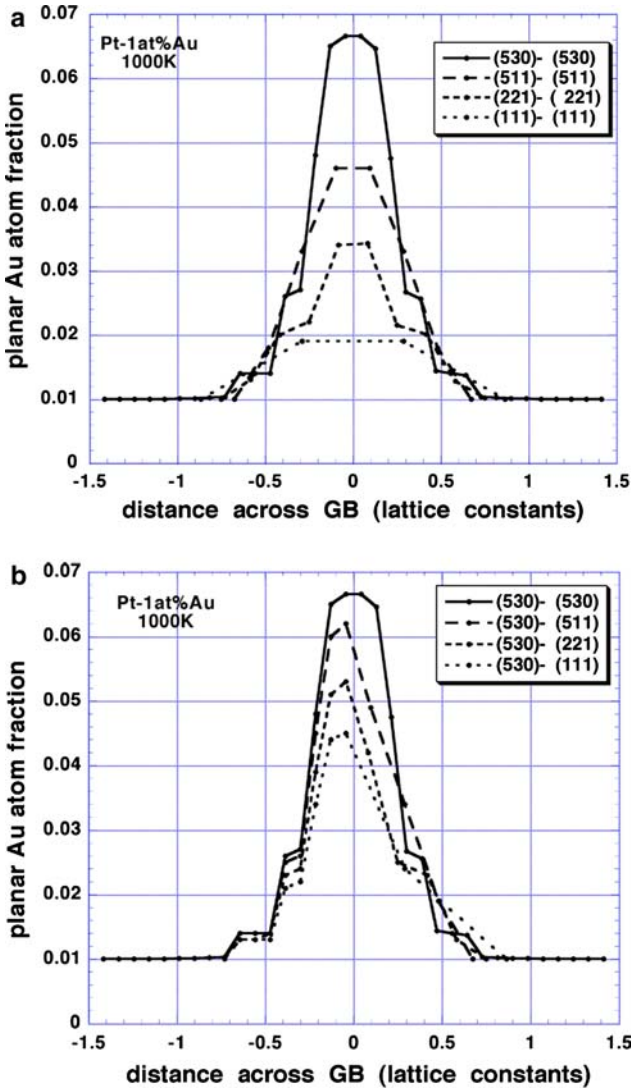

Fig. 4 Composition profiles across GB's in Pt-1 at%Au at 1000 K. In (**a**) the GB's are terminated on identical pairs of planes, and in (**b**) all GB's are terminated by a (530) plane on the left, and by (530), (511), (221) and (111), respectively, on the right

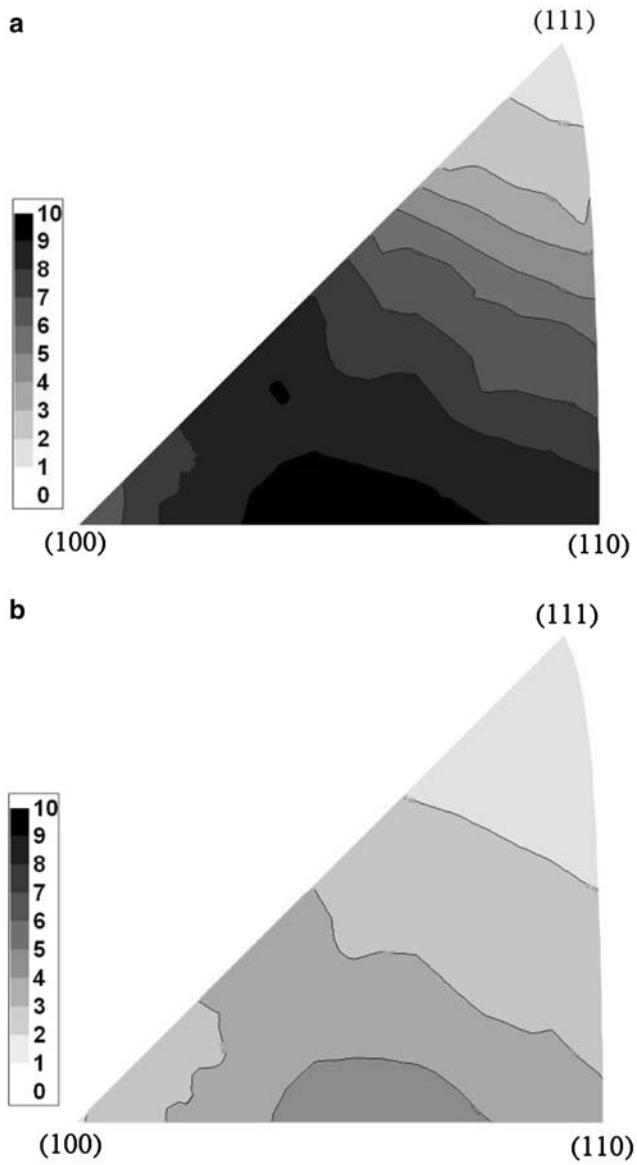

Fig. 5 Distribution of Au adsorption (atoms/nm^2) in Pt-1 at%Au at 400 K (**a**) on one side of the GB for GB's terminated on both sides by the same (*hkl*) orientation, and (**b**) on the (111) side of GB's terminated by the (111) orientation on one side, and all possible orientations on the other side. The scale of the contour plots is in Au atoms/nm^2

(530)–(530), (511)–(511), (221)–(221) and (111)–(111). These profiles are all symmetric, as expected, and the figure shows that segregation is strongest for the (530)–(530) GB and weakest for the (111)–(111) GB. In Fig. 4b, the four GB's shown are comprised of a (530) terminating plane on the left hand side (lhs), whereas the orientation on the right hand side (rhs) is varied through the sequence (530), (511), (221) and (111). The (530)–(530) boundary is of course identical in both figures, and is only shown in Fig. 4b for comparison. It can be seen in Fig. 4b that the composition profile on the (530) side, i.e. lhs of the GB, is dependent on the orientation of the rhs terminating plane. If the rhs plane is characterized by a weak segregation when it is present in a symmetric boundary, as indicated in Fig. 4a, then it also lowers the segregation profile on the (530) side of the GB in Fig. 4b. Similarly, the segregation on the more weakly segregated rhs terminating planes is raised when they are coupled with the strongly segregating (530) plane on the lhs. This provides evidence of the interaction of the segregant atoms across the GB, which comes about in the model from the terms containing the regular solution constant, ω. Thus, the model predicts that in an ideal solution ($\omega = 0$) the composition profile on one side of

the GB would depend only on the orientation of the terminating plane on that side, and would be independent of the orientation of the plane on the other side of the GB. For non-zero values of ω, the degree of compositional interaction will increase with increasing ω.

In order to illustrate the interaction across the GB over a broader range of the orientation parameters than in Fig. 4, we show in Fig. 5a the variation over the standard stereographic triangle of the composition on each side of GB's terminated by identical (hkl) planes, and in Fig 5b, the variation of composition of a terminating (111) plane when the other side of the GB varies over the stereographic triangle. The Pt–1at%Au alloy is still used as the example, but for a temperature of 400 K. Figure 5b illustrates effects similar to those seen in Fig. 4b, namely that the composition of a (111) terminating plane is sensitive to the composition on the other side of the GB, and increases with increasing segregation on the other side. Experimental evidence of such behavior has been found recently at GB's in TiO_2 doped with Nb, as described below.

Experimental results

The results reported here are for a solid solution TiO_2 (rutile) containing 2 mol% Nb_2O_5 [1]. Segregation of Nb to TiO_2 GB's was studied by Auger electron spectroscopy on intergranular fracture surfaces, and the composition of each GB was examined on both sides of the fracture surface. After the Auger measurements, the orientation of each GB fracture surface was determined by combining a stereo-pair method implemented in a scanning electron microscope with orientation imaging microscopy measurements. Details on the experimental techniques and measurements can be found in [1].

Results on 83 GB's (i.e. 166 GB fracture surfaces) are displayed in Fig. 6a in the form of points plotted in the standard stereographic triangle for the tetragonal rutile structure. The location of the points indicate the orientation of the surface normals of the GB fracture planes, and different symbols are used for the points to indicate weak, moderate or strong segregation. Figure 6a shows that the orientation of the GB planes with the strongest segregation lie along the (001)–(011) edge of the triangle, whereas the GB planes with the weakest segregation lie in the vicinity of the (110)–(010) edge of the triangle. Thus there is a clear crystallographic separation of GB planes displaying strong and weak segregation. We will return to this aspect of the results a little later. In Fig. 6b, we replot the orientations of GB planes that show strong segregation, identifying them by solid symbols, and the orientations of the planes of the matching halves of those boundaries denoting them by open symbols. It can be seen that the matching halves of GB planes displaying strong segregation generally also tend to fall in the orientation region that corresponds to strong segregation. This is exactly the behavior we would expect from our previous

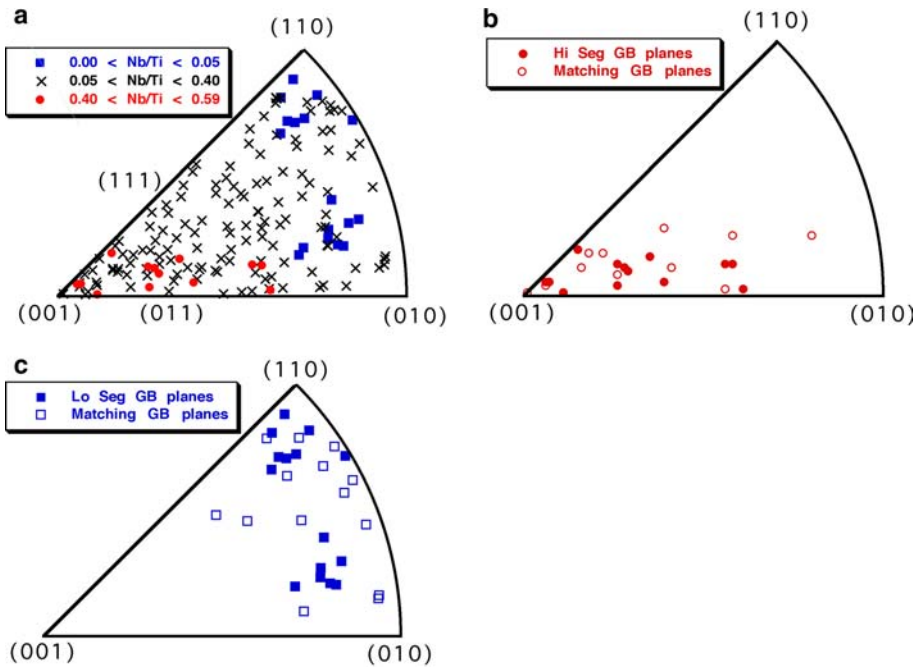

Fig. 6 (**a**) Distribution of GB planes in the standard stereographic triangle for tetragonal TiO_2, showing orientations corresponding to high levels (solid circles) low levels (solid lozenges) and moderate levels of Nb segregation (crosses). (**b**) GB plane orientations with Nb/Ti peak ratios between 0.40 and 0.59 (solid symbols) and the matching planes on the other sides of those grain boundaries (open symbols). (**c**) GB plane orientations with Nb/Ti peak ratios below 0.05 (solid symbols) and the matching planes on the other sides of those grain boundaries (open symbols). After Ref [1]

discussion of Fig. 5, which showed that a boundary plane will tend to display stronger segregation if its matching half also displays strong segregation.

Figure 6c is a plot similar to 6b, but for the case of GB's planes exhibiting weak segregation. In this case, the matching halves of planes with weak segregation, also fall in the orientation region characterized by weaker segregation, thereby confirming the trends predicted by the GB segregation model, and shown in Fig. 5.

Clearly, the present model, which is appropriate for FCC alloys, cannot be expected to yield quantitative segregation predictions for the more complex case of a tetragonal ionic system. Nevertheless, the results obtained from the model provide a reasonable basis for the interpretation of the experimental results.

Wetting transitions at GB's

A regular solution model of wetting transitions in systems consisting of two liquids was developed some time ago [17]. That model was quite similar in form to the present model of GB segregation. It is therefore interesting to determine whether the GB segregation model also predicts the occurrence of wetting transitions at GB's.

It is useful to begin by describing some of the characteristics expected of adsorption behavior in systems displaying wetting transitions [23, 24]. Consider a binary liquid system in which the phase diagram displays a miscibility gap, as shown schematically in Fig. 7a. Liquid B is assumed to have a lower surface energy than liquid A. Under these conditions, a regular solution model would predict an excess of component B at the surface of an A-rich liquid. Now consider the composition trajectory identified in Fig. 7a, in which the composition of an A-rich liquid approaches the two-phase coexistence composition (X_O'), at a temperature above the wetting transition temperature (T_W). Figure 7b shows that the adsorption of B at the surface of the A-rich liquid will increase as the bulk concentration of B is increased, and will tend to diverge as phase coexistence at X_O' is approached. Furthermore, the divergence is expected to display a logarithmic character [25].

In Fig. 8a we present the calculated composition profile across a (210)–(210) GB at 300 K, for Pt–Au alloys containing increasing concentrations of Au. The edge of the miscibility gap on the Pt-rich side occurs at 300 K for an Au atom fraction of $X_O' = 0.106615...$ With increasing Au bulk concentration, Au adsorption at the boundary (which is related to the area under the composition profile) is also seen to increase rapidly as the composition approaches two-phase coexistence. A plot of GB adsorption of Au versus $-\ln(X_O'-X)$ is displayed in Fig. 8b. It shows linear behavior, indicating that the divergence in adsorption as coexistence is approached indeed displays the expected logarithmic character.

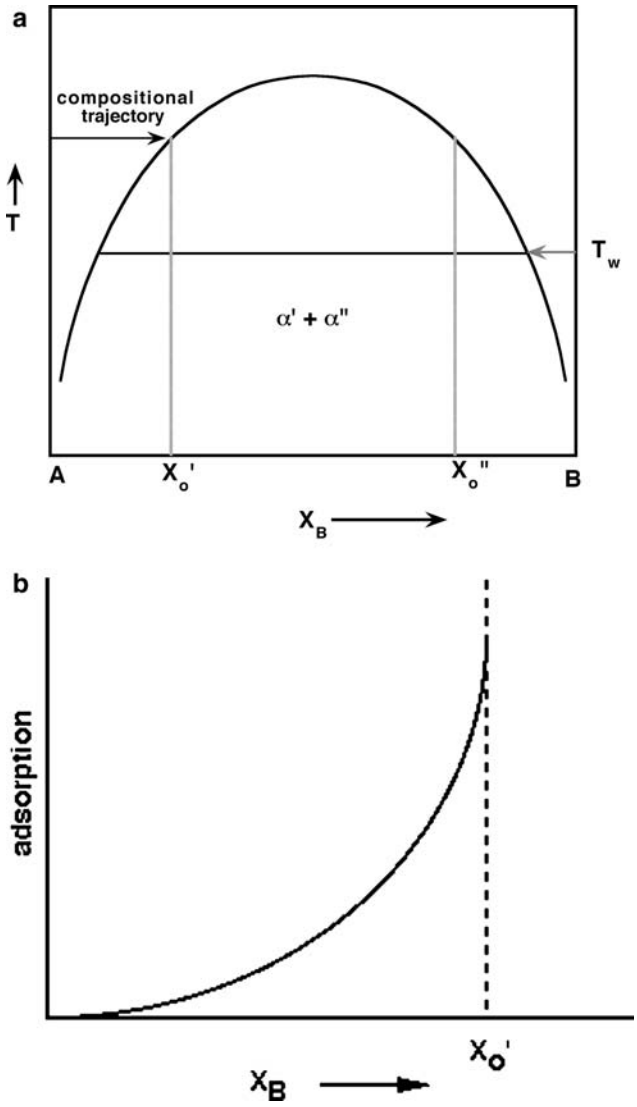

Fig. 7 (**a**) Schematic phase binary diagram of AB system with miscibility gap, where T_W indicates the wetting transition temperature; a composition trajectory terminating at the edge of the miscibility gap is indicated. (**b**) Schematic of the changes in adsorption of B at the surface of the A-rich phase along the trajectory shown in (**a**)

Another feature of the profiles in Fig. 8a is also of interest. It can be seen that as two-phase coexistence is approached, the GB composition profile evolves so as to indicate incipient formation at the boundary of the coexisting phase on the other side of the miscibility gap (α'', of composition X_O'' in Fig. 7a). This manifests

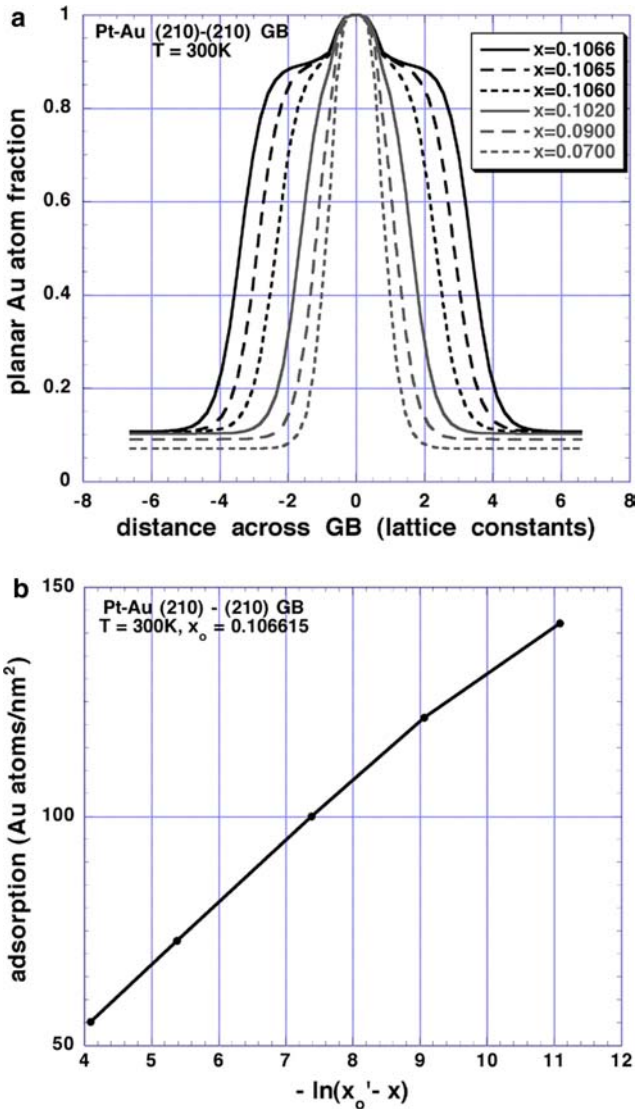

Fig. 8 (**a**) Composition profiles across a (210)–(210) GB for compositions close to the edge of the miscibility gap at $T = 300$ K. (**b**) Au adsorption versus natural log of compositional displacement from the edge of the miscibility gap

itself as a shoulder of composition $X_O'' = 1–X_O' \approx 0.9$, which is separated from the bulk α' by another segment of profile that represents the α'/α'' interface. This incipient formation of the α'' phase at the GB, before the bulk composition has reached the coexistence composition, presages the precipitation of a slab of the α'' phase at the GB when phase coexistence is finally achieved.

In order to illustrate the anisotropy of GB wetting, we show two relevant results. The first, in Fig. 9, shows the composition profiles across of two GB's that differ in orientation from the GB shown in Fig. 8a. Both are terminated on the left by a (210) plane, and by (111) and (511) planes, respectively, on the right. It can be seen that the adsorption is significantly higher on the

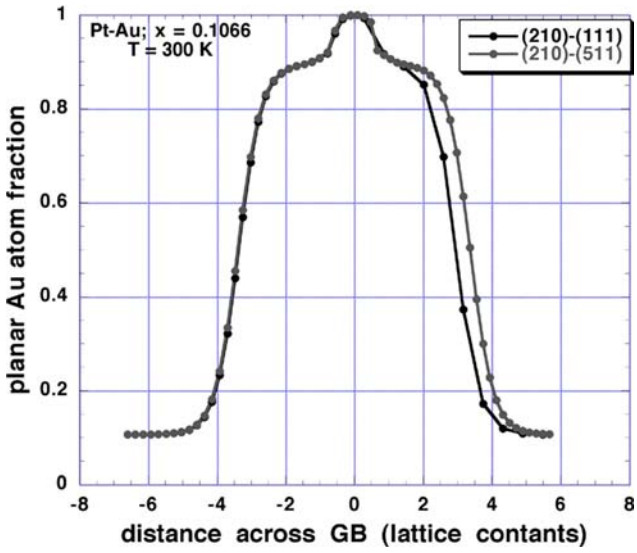

Fig. 9 Composition profiles at $T = 300$ K across (210)–(111) and (210)–(511) GB's for a composition close to the edge of the miscibility gap

(210) side than the (111) side of the (210)–(111) GB, and that the total adsorption of this GB is less than that of the (210)–(511) GB (Fig. 9) and of the (210)–(210) GB (Fig. 8a). Thus the thickness of the incipient α'' phase on each side of a GB depends on the crystallography of the terminating planes.

The second illustration of anisotropy relates to the wetting transition temperature. Figure 10 compares the composition profiles across a (210)–(210) GB and a (111)–(111) GB at a temperature of 250 K, for a bulk

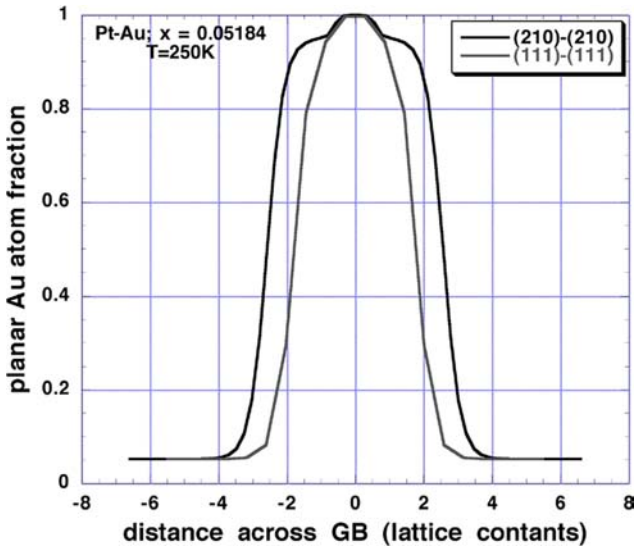

Fig. 10 Composition profiles at $T = 250$ K across (210)–(210) and (111)–(111) GB's for a composition close to the edge of the miscibility gap. Note the presence of α'' precursor shoulders on the (210)–(210) GB profile, and the absence of such shoulders on the (111)–(111) GB profile

Au atom fraction of $X = 0.05184$ (quite close to the coexistence composition of $X_O' = 0.051855...$). Based on the appearance of a shoulder of composition close to $X_O'' \approx 0.95$ on the (210)–(210) GB profile, but not on the profile across the (111)–(111) GB, it is possible to conclude that the wetting temperature for the (210)–(210) GB lies below 250 K, whereas the wetting temperature of the (111)–(111) GB lies above that temperature. Similar calculations performed at 200 K indicate that this temperature is below the wetting temperature of both (210)–(210) and (111)–(111) GB's. Thus, these calculations show that the wetting temperature is anisotropic, and that this anisotropy may be estimated from the GB segregation model. More work along these lines is needed in order to gain a better picture of the extent of wetting anisotropy, and of its dependence on various model parameters.

The above results provide evidence that the GB segregation model is capable of predicting wetting transitions at GB's, but should be accepted with caution. The model, as presented here, is only suitable for describing solid–solid equilibria. While transitions involving wetting of a GB by a solid phase are possible, they are only expected to occur if the interface between the equilibrium α' and α'' phases is coherent [26]. This places significant restrictions on the possibility of solid–solid wetting transitions, although it is worth mentioning that a transition from discrete to slab-like Al precipitation has been observed at GB's in Al–Zn alloys [12].

Thus far, the GB segregation model has not been extended to equilibria involving GB's with a liquid phase. In view of the interest in the phenomenon of GB wetting by a liquid phase, e.g. in the context of liquid metal embrittlement, an extension of this type of model to account for both solid–liquid equilibria as well as GB segregation would certainly be a worthwhile goal.

Conclusions

We have exercised a recently developed model of GB segregation, which is suitable for exploring GB properties as a function of the five macroscopic parameters of GB orientation. The model has been applied to the case of a Pt–1at%Au FCC alloy, in which Au segregates to the GB's. The model predicts several interesting trends. The equilibrium composition as well as the composition profile, on one side of a boundary with a given terminating plane, depends on the crystallographic orientation of the terminating plane on the other side of the GB. Experimental results confirming these predictions are drawn from recent measurements of GB segregation in TiO_2 performed on 83 matching pairs of GB fracture surfaces.

In addition, it has been shown that the GB segregation model is able to predict the presence of solid-state GB wetting transitions, which display the expected logarithmic divergence of adsorption as two-phase coexistence is approached. Finally, it has been shown that GB's of different orientations are characterized by different wetting transition temperatures, and that the thickening of precursing wetting layers is also anisotropic.

Acknowledgements PW and YP wish to acknowledge with thanks support of their research by the MRSEC Program of the National Science Foundation under award DMR-0079996. DC acknowledges with thanks support of her research by the COOLCOP project of the European Space Agency.

References

1. Pang Y, Wynblatt P (2005) J Am Ceram Soc 88:2286
2. Pang Y, Wynblatt P (2006) J Am Ceram Soc 89:666
3. Wolf D (1989) Acta Metall 37:1983
4. Wolf D (1989) Acta Metall 37:2823
5. Wolf D (1990) Acta Metall Mater 38:791
6. Seidman DN (2002) Annu Rev Mater Res 32:235
7. Wynblatt P, Shi Z (2005) J Mater Sci 40:2765
8. Bishop CM, Cannon RM, Carter WC (2005) Acta Mater 53:4755
9. Tang M, Carter WC, Cannon RM (2006) Phys Rev B 73(2):24102
10. Wynblatt P, Takashima M (2001) In: Eustathopoulos N, Nogi K, Sobczak N (eds), Proceedings of HTC-2000, Trans JWRI 30:11
11. Wynblatt P, Takashima M (2001) Interface Sci 9:265
12. López GA, Mittemeijer EJ, Straumal BB (2004) Acta Mater 52:4537
13. Avishai A, Sheu C, Kaplan WD (2005) Acta Mater 53:1559
14. Avishai A, Kaplan WD (2005) Acta Mater 53:1571
15. Mclean D (1957) Grain boundaries in metals. Oxford Press, London
16. Wynblatt P, Ku RC (1979) In: Johnson WC, Blakely JM (eds), Interfacial segregation. ASM, Metals Park, Ohio, p 115
17. Wynblatt P, Saul A, Chatain D (1998) Acta Mater 46:2337
18. Lee YW, Aaronson HI (1980) Surface Sci 95:227
19. Lee YW, Aaronson HI (1980) Acta Metall 28:539
20. Udler D, Seidman DN (1992) Phys Stat Sol B 172:267
21. Udler D, Seidman DN (1994) Acta Metall Mater 42:1959
22. Foiles SM, Baskes MI, MS Daw (1986) Phys Rev B33:7983
23. Cahn JW (1977) J Chem Phys 66:3667
24. Schick M (1990) In: Charvolin J, Joanny JF, Zinn-Justin J (eds), Liquids at interfaces. Elsevier, Amsterdam, p 415
25. Widom B (1978) J Chem Phys 68:3878
26. Cahn JW (2000) Physica A 279:195